JOURNAL OF MATERIALS SCIENCE 30 (1995) 4669–4675

Crack layer analysis of fatigue crack propagation in ABS polymer

T. J. BOHATKA, A. MOET*
Department of Macromolecular Science, The Case School of Engineering, Case Western Reserve University, Cleveland, OH 44106, USA

Differences in damage formation during fatigue crack propagation in acrylonitrile–butadiene–styrene polymer, between tests both fulfilling and not fulfilling linear elastic fracture mechanics requirements, were related to differences in crack propagation behaviour through the crack layer (CL) theory. At both test conditions, damage consisted of crazing and shear yielding of the matrix, as well as elongation of rubbery domains. For a given crack length, the lower load level showed a higher intensity of craze damage. CL analysis showed that the process-dependent dissipation coefficient, β, is inversely proportional to the lifetime. Further, despite drastic differences in the amounts of each damage species, both tests were estimated to have the same specific enthalpy of damage ($\gamma^* = 105\ \text{cal g}^{-1}$), a material constant that is a measure of the intrinsic resistance to damage formation at the crack tip.

1. Introduction

The advantages of acrylonitrile–butadiene–styrene (ABS) polymers make them viable candidates for many engineering applications, which in turn necessitates reliable data on their fatigue crack propagation (FCP) resistance. The availability of such a reliable data base would facilitate forecasting of field performance and would expedite material development for demanding applications. The majority of published FCP data are plotted in terms of the Paris equation, i.e.

$$\frac{da}{dN} = A(\Delta K)^m \tag{1}$$

where da/dN is the rate of FCP and ΔK is the stress intensity factor range. A and m are empirical parameters which could be transferable to other load-geometry configurations provided linear elastic fracture mechanics (LEFM) dominance is established [1–3].

Examination of the FCP data reported in the literature on ABS reveals that one cannot find unique Paris parameters, A and m. The A and m values of ABS calculated from Paris plots found in two different publications [4, 5] are $4.04 \times 10^{-6}\ \text{m s}^{-1}$ $(\text{MPa m}^{0.5})^{-2.7}$ and 2.7, and $1.3 \times 10^{-7}\ \text{m s}^{-1}$ $(\text{MPa m}^{0.5})^{-3.4}$ and 3.4, respectively. The vastly different A and m values preclude their use as a means for comparing the performance of ABS to other polymers and misguides material development efforts. A primary reason for such a discrepancy is that FCP test results are commonly reported without assurance of compliance with LEFM (K-dominance), a rudimentary requirement for using an LEFM parameter (ΔK) as a similitude parameter. In an earlier publication [6], we have defined the conditions for K-dominant FCP and established a criterion according to which A and m could be considered transferable.

Even though the acquisition of valid A and m is useful in forecasting long-term service performance of components with a known stress intensity factor, they are of limited value in material development. The latter task requires parameters which can be readily related to molecular and microstructural parameters through the damage mechanisms by which the material resists crack propagation. The objective of this paper is to apply the crack layer (CL) theory to deduce the specific enthalpy of damage and the dissipation coefficient, which reflects the viscoelastic character of the material.

2. The crack layer model

Based on the concepts of irreversible thermodynamics, the rate of crack propagation is derived as [7]

$$\frac{da}{dN} = \frac{\beta W_i}{\gamma^* R_1 - J_1} \tag{2}$$

where β is the dissipation coefficient expressed as the fraction of irreversible work (per cycle), W_i expended on the formation of crack tip (damage) plasticity, R_1 is the volume (or mass) of crack tip plasticity (resistance moment), γ^* is the specific enthalpy of

*Author to whom all correspondence should be addressed.

damage, a material constant characteristic of its intrinsic resistance to crack energy release rate.

Qualitatively, Equation 2 can be interpreted in the following way. The numerator expresses an energy "pump" that supplies mechanical work per cycle, βW_i, which causes the accumulation of plastic transformation whose magnitude is R_1. The balance of the irreversible work, i.e., $(1-\beta)W_i$, is assumingly dissipated as heat. Obviously, R_1 represents the material resistance to crack growth and is thus called the "resistance moment". If γ^* is the specific enthalpy of crack tip transformation, the product $\gamma^* R_1$ is the resistance energy. J_1 is the driving energy. With time, R_1 increases until $\gamma^* R_1$ can no longer resist J_1. At this moment, the "energy barrier", $\gamma^* R_1 - J_1$ approaches zero and the crack "jumps" into the plastic zone. Provided the requirements for global instability (catastrophic failure) are not yet met, the crack will then halt, to allow for another sequence of crack tip deformation followed by fast crack excursion. These are considered as local instabilities which are repeated until ultimate failure occurs.

In contrast to the Paris equation, the CL theory does not demand conformity to linear or non-linear fracture mechanics, nor does it require the dominance of a particular stress state [8]. In fact, Equation 2 will be employed to relate damage mechanisms to FCP behaviour for both a test that is compliant with LEFM ($\sigma_{max} = 5.0$ MPa), and one that is not ($\sigma_{max} = 10.8$ MPa). Again, details of LEFM analysis of these data have been reported elsewhere [6].

3. Experimental procedure

The ABS used in this study was received from the Dow Chemical Company in the form of injection-moulded plaques. Tensile testing at a strain rate of 25% min^{-1} determined the yield stress to be 46 MPa.

Specimens were cut from the injection-moulded plaques and machined into rectangular, SEN specimens of dimensions 25.4 mm × 3.3 mm with a gauge length of 102 mm. A 60° notch was then machined into the edge to a depth of 2.54 mm and then finished off with a razor blade to a total notch depth of 3.5 mm.

The fatigue testing was done using an MTS servohydraulic machine. The loading was tension–tension using a sinusoidal waveform. The frequency was kept at 1 Hz to avoid hysteretic heating. The R-ratio ($\sigma_{min}/\sigma_{max}$) was maintained at 0.1 so that creep ($R = 1$) was minimized. All tests were performed under ambient conditions at room temperature. The maximum load level, σ_{max}, was the testing variable and was set at values of 5.0 and 10.8 MPa (11% and 23% of the yield stress, respectively).

Throughout each test, the crack length was followed with a travelling microscope to a resolution of 0.25 mm. Load–displacement loops were also acquired at selected crack extensions.

For each of the two loading conditions, four or five tests were interrupted at different crack lengths for damage zone analysis. The crack lengths at which FCP was interrupted were more or less evenly spaced along the specimen width. Serial sections of the damage zones were then prepared in a plane perpendicular to the specimen width, 60 μm per pass, using a Jung Frigocut 2800E at − 40 °C. The sections of the damage zones were then placed between glass slides and viewed with an optical microscope and photographed under transmitted light.

Ultra-thin sections were microtomed following the method prescribed by Dillon and Bevis [9]. A Jeol JEM-100SX transmission electron microscope was used to view the samples. To prevent scorching of the sample, the intensity of the electron beam was maintained relatively diffuse.

4. Results and discussion

The goal of this study was to relate damage mechanisms to FCP behaviour for both the test that is compliant with LEFM and gives transferable Paris parameters ($\sigma_{max} = 5.0$ MPa), and the one that is not ($\sigma_{max} = 10.8$ MPa). In the formalism of the crack layer theory, the damage zone is related to the crack speed through Equation 2. From here, the approach taken will be to determine each of the experimental parameters of Equation 2, (i.e. da/dN, W_i, R_1, and J_1), as a function of crack length for each loading condition. The specific enthalpy of damage and the dissipation coefficient will then be determined from the fit of Equation 2 to the experimentally determined parameters.

4.1. Crack velocity

In Fig. 1, the crack length is plotted against the number of cycles for fatigue tests of $\sigma_{max} = 10.8$ and 5.0 MPa. The data show the crack length to increase monotonically as a function of time (number of cycles), until catastrophic failure. As expected, the higher σ_{max} test reaches a higher crack length in a given number of cycles. Also, the higher σ_{max} test has a lower critical crack length.

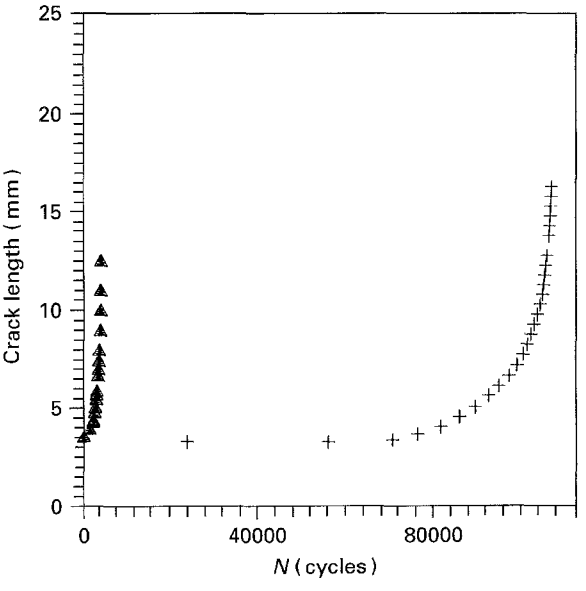

Figure 1 Crack length versus number of cycles for σ_{max} = (+) 5.0 and (▲) 10.8 MPa.

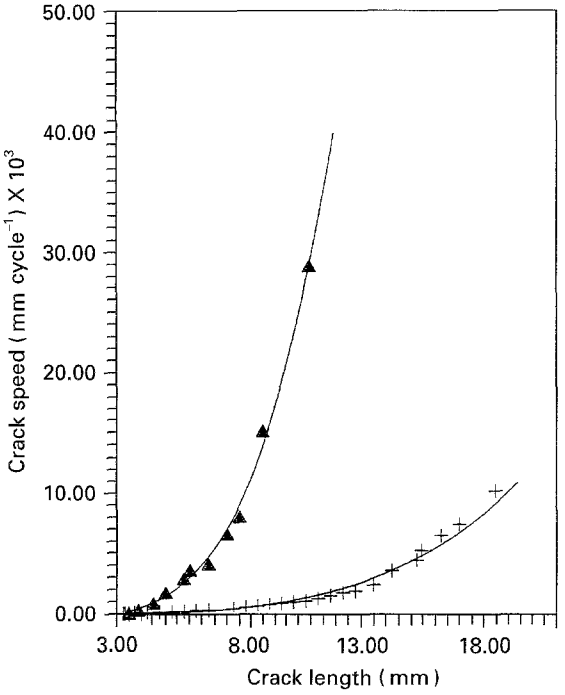

Figure 2 Crack speed versus crack length for the two load levels tested: (+) 5.0 MPa, (▲) 10.8 MPa.

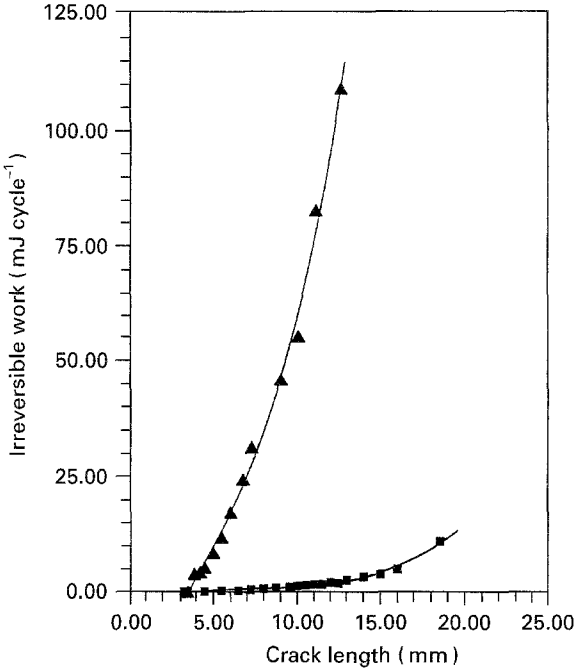

Figure 3 Irreversible work versus crack length for the two load levels tested: (■) 5.0 MPa, (▲) 10.8 MPa.

FCP has been reported to occur in a discontinuous manner, by the development of, and subsequent propagation through, a damage zone [10]. As a result, care must be taken in deriving a continuous function for crack speed from this discontinuous process. In this experiment, the crack length was measured to a resolution of 0.25 mm and the crack speed was found by a finite difference method in which the slope of the a versus N curve was found at particular values of crack length. To ensure the accuracy of the calculated slope, many data points were taken in the a versus N curve (every 0.25 mm) so that the finite slope approached the derivative of this curve. The resulting plot of da/dN versus a is shown in Fig. 2.

4.2. Irreversible work

The irreversible work expended per cycle is found as the area within a load–displacement hysteresis loop minus the area of the first loop recorded, which accounts for the natural hysteresis of the specimen. Fig. 3, as expected, shows that at any given crack length, the irreversible work is higher for the higher stress test. This is produced by both the higher load level and the accompanying larger displacement.

4.3. Energy release rate

The energy release rate, J_1, is found as the negative of the change in the potential energy, P, with crack length, i.e.

$$J = -\frac{1}{t_0}\frac{dP}{da} \tag{3}$$

The potential energy was determined by a method similar to that outlined by Begley and Landes [11]. In order to account for any crack advance that might occur during the loading stroke, the potential energy was taken as the area above the unloading curve of the hysteresis loop. A third-order polynomial function provided an excellent fit to the data and the derivative of this fit equation was calculated and used in Equation 3 to obtain J.

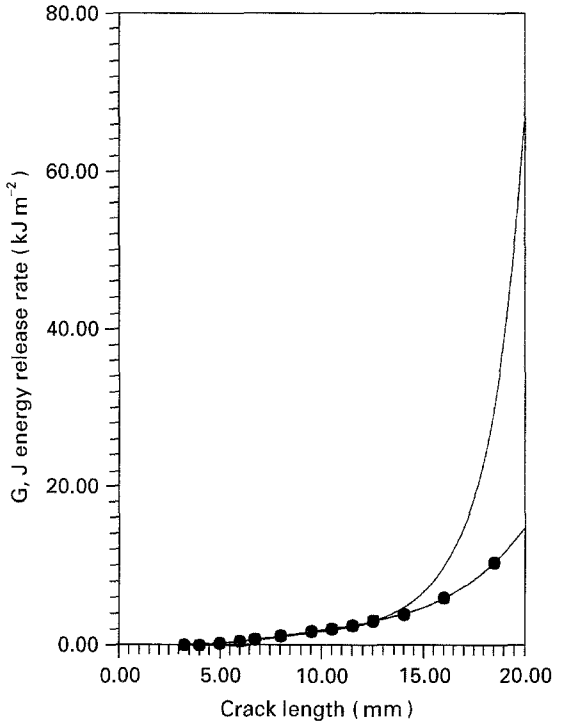

Figure 4 Energy release rates, (–) G and (●) J, versus crack length for the test of σ_{max} = 5.0 MPa.

The resulting plots of J versus crack length are shown in Figs 4 and 5 together with the LEFM-based energy release rate, i.e. $G_1 = K^2/E'$ [12]. Curiously, it is noticed that G_1 initially agrees with J_1, but then exceeds it at higher crack lengths. Although the

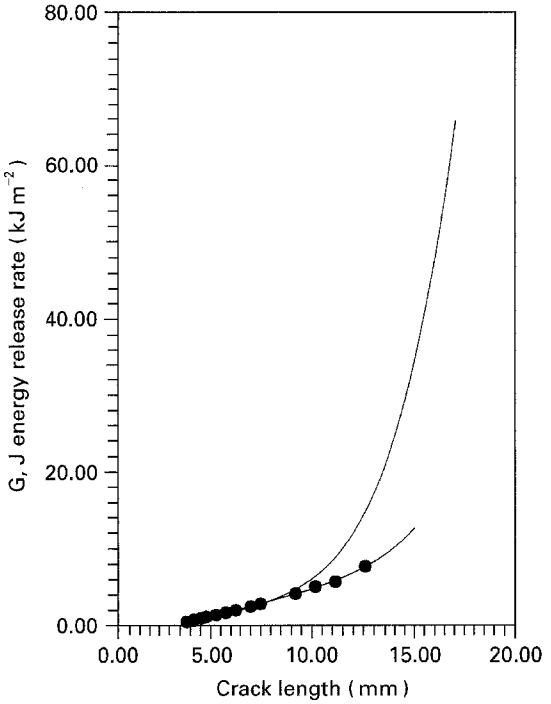

Figure 5 Energy release rates, (—) G and (•) J, versus crack length for the test of $\sigma_{max} = 10.8$ MPa.

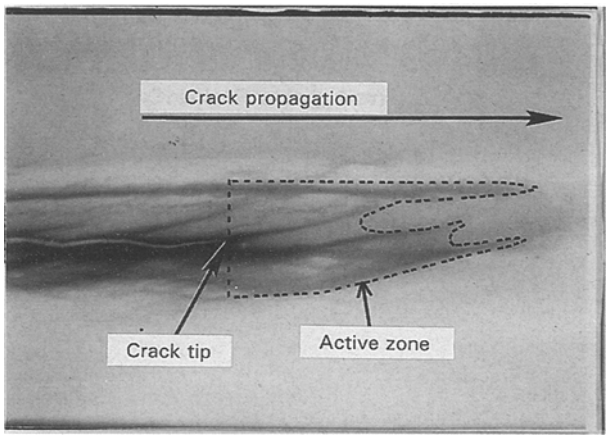

Figure 6 Transmitted light micrograph of a typical damage zone at the specimen surface (× 15), ($\sigma_{max} = 10.8$ MPa and crack length is 13 mm).

underlying reason for this remains to be seen, the same phenomenon has been previously observed in many different polymers [13–18].

4.4. Resistance moment

To determine the resistance moment, the damage ahead of the crack tip must be identified and then measured. Fig. 6 illustrates the active zone containing stress-whitened material as seen from a side view at the specimen surface. The evolution of the volume of this damage zone as a function of crack length is shown in Fig. 7. As expected, the damage (plastic zone) volume increases more rapidly for the higher stress level [12]. However, it is the damage detail within this volume that is responsible for the resistance to crack propagation.

TEM analyses [19] indicate that the damage zone consists of crazing, shear yielding, and deformation of

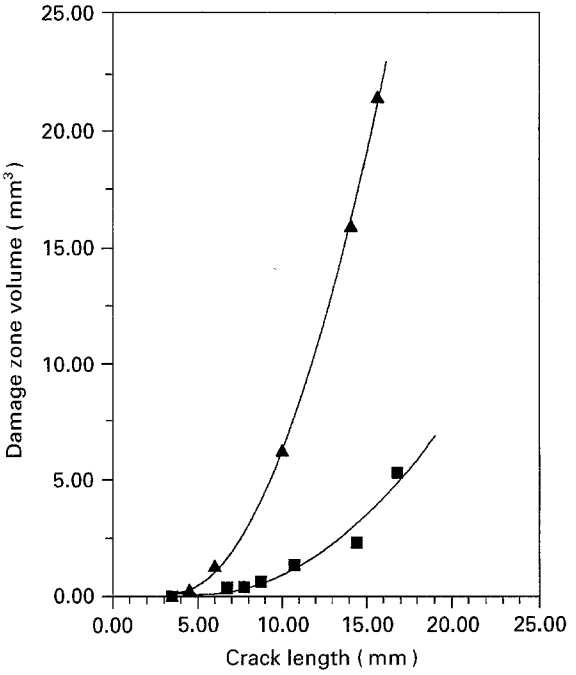

Figure 7 Total damage zone volume versus crack length for the two load levels tested: (■) 5.0 MPa, (▲) 10.8 MPa.

rubbery domains (Fig. 8a and b). The latter two are interrelated and, therefore, the intensity of one should account for the intensity of the other. Hence, only crazing and rubber domain deformation will be considered in the quantitative damage analysis to compute the resistance moment. The methods used to determine each contribution are outlined below. Thus, the resistance moment will be considered as the sum of the two contributions, i.e.

$$R_1 = R_c + R_{r/m} \quad (4)$$

where R_1 is the total resistance moment, R_c is the craze contribution, and $R_{r/m}$ accounts for the shear contribution of the rubbery domains and matrix.

4.4.1. Crazing of the matrix

Fig. 8a and b show typical transmission electron micrographs taken from the damage zone at the two stress levels. The difference in craze size and number are apparent. At the lower stress level (Fig. 8a), the crazes are wider and more numerous. This observation reflects the time-dependent character of craze initiation and growth. At low load level, the crack tip zone experiences stress and strain over a much longer time period. Indeed, Fig. 1 shows that the time to reach a given crack length is vastly greater at the lower load level. This allows more crazes to initiate and grow. Similar findings have been reported as a function of strain rate for monotonically tested SAN [20].

To quantify the contribution of crazes to the resistance moment, the following steps have been taken. First, the number of crazes per unit area, N_c/A, and the average craze width, W_c, were determined by image analysis (Table I). Together with the fact that the average craze length was found to be 0.64 μm, the volume fraction of crazes within the damage zone,

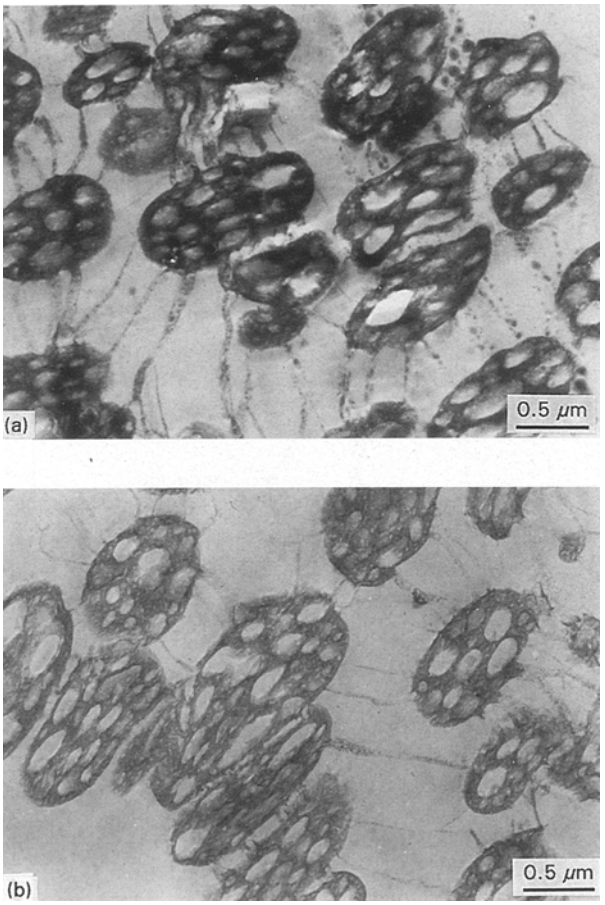

Figure 8 Transmission electron micrographs of the deformed sample: (a) $\sigma_{max} = 5.0$ MPa and $a = 10$ mm; (b) $\sigma_{max} = 10.8$ MPa and $a = 10$ mm.

TABLE I Average craze width, w_c, average number of craxes per unit areas, $N_c\ \mu m^{-2}$, and volume fraction of crazes, ϕ_c, for $\sigma_{max} = 5.0$ and 10.8 MPa (crack length = 10 mm)

σ_{max} (MPa)	$W_c(\mu m)$	$N_c(\mu m^{-2})$	ϕ_{craze}
5.0	0.197	6.04	0.76
10.8	0.053	1.94	0.07

ϕ_{craze}, was calculated. Assuming the volume fraction of fibrillar material within the craze to be 0.55 [21], and the density of SAN to be $1.1\ g\,cm^{-3}$ [22], the resistance moment for craze damage, R_c, within the damage zone is computed and plotted as a function of crack length (Fig. 9). Note the inversion of the relative magnitude of craze damage between the two load levels as compared to that of the total damage volume (Fig. 7).

4.4.2. Deformation of the rubber domains

Fig. 8a, b show that for both the $\sigma_{max} = 5.0$ and 10.8 MPa tests, elongation of the rubber domains accompanies the crazing. Although not obvious, image analysis has revealed that the average aspect ratio of the rubbery domains is slightly greater at the lower load level ($\sigma_{max} = 5.0$ MPa) than at the higher load level ($\sigma_{max} = 10.8$ MPa) (Table II). It is estimated that these aspect ratios correspond to strain levels in the

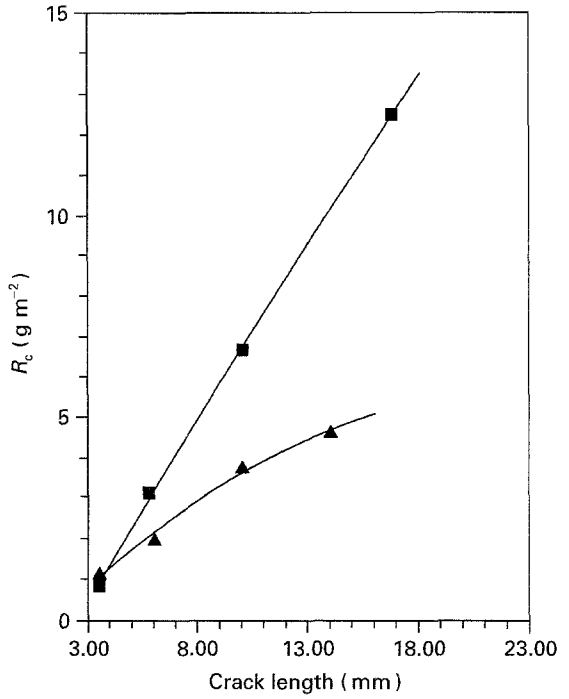

Figure 9 R_c versus crack length for the two load levels tested: (■) 5.0 MPa, (▲) 10.8 MPa.

TABLE II The weighting factor for the intensity of rubber elongation, χ, for both load levels tested

σ_{max} (MPa)	Aspect ratio	χ
5.0	2.49	3.64
10.8	2.21	2.22

rubbery domains in excess of 100%. This reflects the coupled deformation behaviour of the multiphase system within the plastic zone.

To quantify the contribution of rubbery deformation to the resistance moment, the following steps are taken. First, the fractional area of the rubbery domains within the damage zone was determined. The intensity of damage associated with the deformation of rubbery domains has been assumed to scale with the local strain. A scaling factor, χ, was computed for both load conditions and is shown in Table II. Knowing the volumetric contribution, and taking the density of butadiene rubber as $1.2\ g\,cm^{-3}$ [22], the resistance moment for deformation of the rubbery domains, $R_{r/m}$, is computed and plotted as a function of crack length (Fig. 10).

4.4.3. Calculation of the resistance moment

The resistance moment computed from Equation 4 in accordance with the preceding analysis is shown in Fig. 11. At the notch tip, prior to crack initiation, the amount of damage is expectedly higher at the higher stress level. Also, the rate of damage evolution with crack length is greater. As the resistance moment analysis accounts for the detailed damage processes, its behaviour displays notable differences from the behaviour of the plastic zone volume (Fig. 7). It should

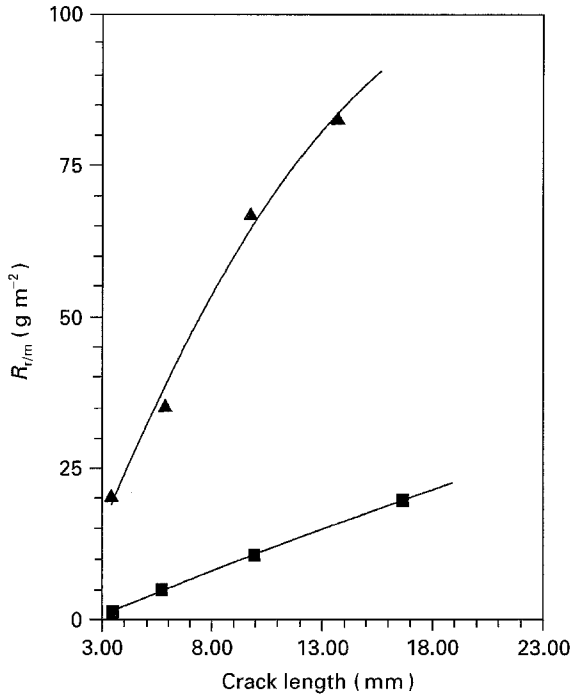

Figure 10 $R_{r/m}$ versus crack length for the two load levels tested: (■) 5.0 MPa, (▲) 10.8 MPa.

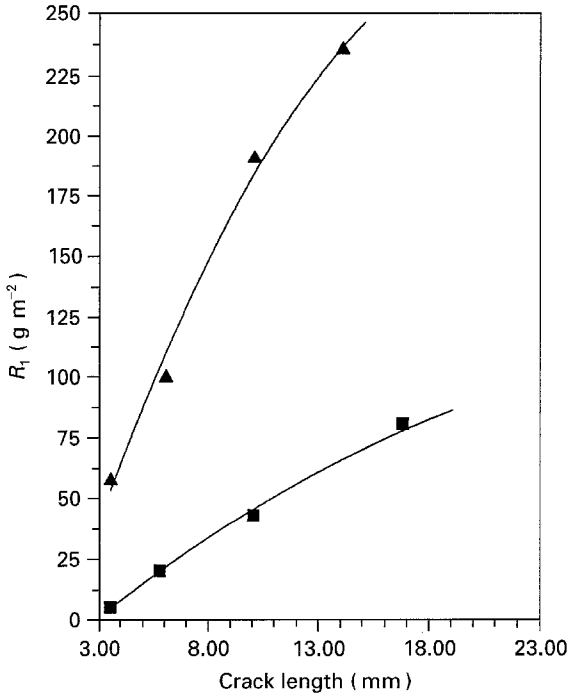

Figure 11 R_1 versus crack length for the two load levels tested: (■) 5.0 MPa, (▲) 10.8 MPa.

be noted that the relative contributions of crazing and rubber domain deformation were assumed to remain unaltered during crack propagation. In view of the self-similarity that is known to dominate crack-tip plasticity, this assumption seems adequate.

4.5. Linearized crack layer fit

With all of the experimentally measurable variables in Equation 2 determined, it is now rearranged into a linear form to facilitate determination of γ^* and β

$$\frac{J}{R} = \gamma^* - \beta \frac{W_i}{Rt_0 da/dN} \quad (5)$$

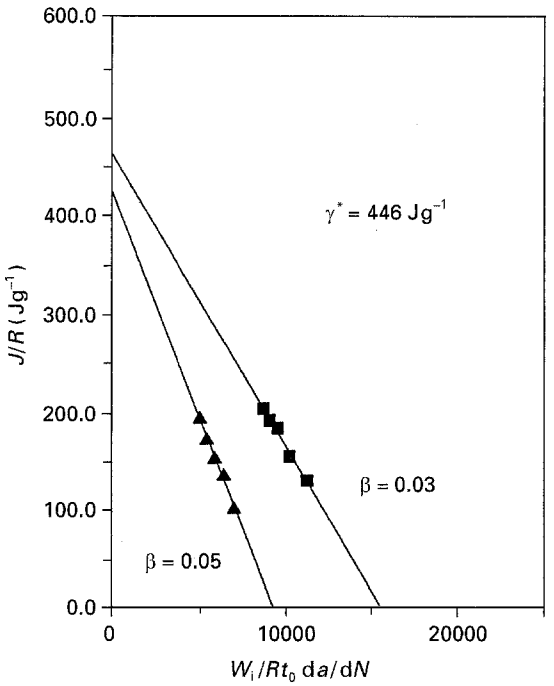

Figure 12 Linearized crack layer fit showing the resulting values of γ^* and β for (■) 5.0 MPa and (▲) 10.8 MPa.

TABLE III Values of γ^*, β, and the total lifetime, N_f, for the two load levels tested

σ_{max} (MPa)	γ^* (cal g^{-1})	β	N_f(cycles)
5.0	111	0.03	106000
10.8	102	0.05	3920

By plotting J/R against $W_i/(Rt_0 da/dN)$, the constants γ^* and β are obtained as the y-intercept and slope, respectively (Fig. 12). The resulting values of γ^* and β are shown in Table III. In spite of the gross assumptions invoked in the calculation of R_1 associated with complex, interacting damage processes within the active zone, a nearly constant value of γ^* is obtained at ~ 450 J g^{-1} (105 cal g^{-1}).

One notices that β is larger at the higher load level than it is at the lower load level. The fact that a larger portion of the energy per cycle is expended on damage processes than dissipated as heat (see Section 2) indicates that the use of energy to form damage is more efficient. In this way, it seems appropriate that for the higher load level, the higher β correlates with a decrease in the specimen lifetime (Table III). A similar correlation has been noted for other materials.

As suggested by the CL theory, the specific enthalpy of damage, γ^*, measures the intrinsic (time-independent) resistance to crack propagation. On the other hand, β is a process-dependent parameter that contains information about the viscoelastic character of the material. Though γ^* and β must be considered together, it is informative to compare various γ^* for different polymers (Table IV). It is noticed that a PC/ABS blend exhibits a synergistic effect, as the γ^* for the blend exceeds those of its components. The work presented here provides evidence that the fatigue

TABLE IV Comparison of γ^* of ABS with that of other commonly used polymers

Material	γ^* (cal g^{-1})
ABS	105
PC/ABS [13]	160
PS [14]	15
PC [15]	10–15
PET [16]	0.35
RTPU [17]	62
HDPE [18]	1–2

resistance of ABS derives from cooperative deformation on the scale of the microstructure.

5. Conclusion

Differences in the FCP behaviour of ABS between a test fulfilling LEFM conditions ($\sigma_{max} = 5.0$ MPa) and one not fulfilling LEFM conditions ($\sigma_{max} = 10.8$ MPa) have been related through the crack layer theory. For both test conditions, the damage formation ahead of the crack tip consisted of crazing and shear yielding of the SAN matrix as well as elongation of rubbery domains. The intensity of crazing and deformation of the rubbery domains was considerably higher in the test fulfilling LEFM. In spite of the differences in the intensity of damage between these different damage species, a single specific enthalpy of damage is obtained for both tests (~ 105 cal g^{-1}). The process-dependent dissipation coefficient, β, was found to rank the fatigue lifetime between the two test conditions.

References

1. M. F. KANNINEN and P. E. O'DONOGHUE, *Eng. Fract. Mech.* **36** (1990) 903.
2. A. OLICK and A. MOET, in "Proceedings of the Thirteenth International Plastic Fuel Gas Pipe Symposium" edited by L. Ingels and R. Olsen, San Antonio, TX (American Gas Association, 1993) p. 280.
3. E. SHOWAIB, PhD thesis, Case Western Reserve University, Cleveland, OH (1993).
4. R. W. HERTZBERG, H. NORDBERG and J. A. MANSON, *J. Mater. Sci.* **5** (1970) 524.
5. R. W. HERTZBERG, J. A. MANSON and W. C. WU, ASTM STP 536 (American Society for Testing and Materials, Philadelphia, PA, 1973) p. 396.
6. T. J. BOHATKA and A. MOET, *Exp. Mech.* to be published (1994).
7. A. CHUDNOVSKY and A. MOET, *J. Mater. Sci.* **20** (1985) 630.
8. J. J. STREBEL and A. MOET, *Polym. Eng. Sci.* **33** (1993) 217.
9. M. DILLON and M. BEVIS, *J. Mater. Sci.* **17** (1982) 1895.
10. A. J. MCEVILY Jr, C. BOETTNER and T. L. JOHNSTON, in "Fatigue – an interdisciplinary approach", edited by J. J. Burke, N. L. Reed and V. Weiss (Syracuse University Pren, Syracuse, NY, 1964) p. 95.
11. J. A. BEGLEY and J. D. LANDES, in "Fracture Toughness, Proceedings of the 1971 National Symposium on Fracture Mechanics", Part II, ASTM STP 514 (American Society for Testing and Materials, Philadelphia, PA, 1972) pp. 1–20.
12. D. BROEK, "Elementary engineering fracture mechanics" (Martinus Nijhoff, 1986).
13. S. R. SEIBEL, MS thesis, Case Western Reserve University, Cleveland, OH (1992).
14. J. BOTSIS, A. CHUDNOVSKY and A. MOET, *Int. J. Fract. Mech.* **33** (1987) 277.
15. N. HADDAOUI, A. CHUDNOVSKY and A. MOET, *Polymer* **27** (1986) 1377.
16. J. KREY, K. FRIEDRICH and A. MOET, *Polymer* **29** (1988) 1433.
17. V. TANRATTANAKUL, MS thesis, Case Western Reserve University, Cleveland, OH (1992).
18. M. L. KASAKEVICH, A. MOET and A. CHUDNOVSKY, *Polymer* **31** (1990) 435.
19. T. J. BOHATKA, MS thesis, Case Western Reserve University, Cleveland, OH (1993).
20. A. M. DONALD and E. J. KRAMER, *J. Mater. Sci.* **17** (1982) 1765.
21. R. P. KAMBOUR, "A review of crazing and fracture in thermoplastics" (General Electric Coy., Schenectady, NY, 1972).
22. H. F. MARK, N. M. BIKALES, C. G. OVERBERGER, G. MENGES and J. I. KROSCHWITZ, "Enclyclopedia of polymer science and engineering" (Wiley, New York, 1990).

Received 31 January
and accepted 4 October 1994